Spin-driven phase transitions in ZnCr2Se4 and ZnCr2S4 probed by high-resolution synchrotron x-ray and neutron powder diffraction

F. Yokaichiya, Alexander Krimmel, Vladimir Tsurkan, I. Margiolaki, P. Thompson, H. N. Bordallo, A. Buchsteiner, N. Stüßer, D. N. Argyriou, Alois Loidl

Spin-driven phase transitions in $ZnCr_2Se_4$ and $ZnCr_2S_4$ probed by high-resolution synchrotron x-ray and neutron powder diffraction

F. Yokaichiya,[1] A. Krimmel,[2] V. Tsurkan,[2,3] I. Margiolaki,[4] P. Thompson,[4] H. N. Bordallo,[1] A. Buchsteiner,[1] N. Stüßer,[1] D. N. Argyriou,[1] and A. Loidl[2]

[1]*Helmholtz Center Berlin for Materials and Energy (formally known as the Hahn-Meitner-Institut), Glienicker Straße 100, Berlin D-14109, Germany*
[2]*Experimental Physics V, Center for Electronic Correlations and Magnetism, Augsburg University, D-86159 Augsburg, Germany*
[3]*Institute of Applied Physics, Academy of Sciences of Moldova, MD2028 Chisinau, Republic of Moldova*
[4]*European Synchrotron Radiation Facility, BP 220, F-38043 Grenoble Cedex, France*

The crystal and magnetic structures of the spinel compounds $ZnCr_2S_4$ and $ZnCr_2Se_4$ were investigated by high-resolution powder synchrotron and neutron diffraction. $ZnCr_2Se_4$ exhibits a first-order phase transition at $T_N=21$ K into an incommensurate helical magnetic structure. Magnetic fluctuations above T_N are coupled to the crystal lattice as manifested by negative thermal expansion. Both the complex magnetic structure and the anomalous structural behavior can be related to magnetic frustration. Application of an external magnetic field shifts the ordering temperature and the regime of negative thermal expansion toward lower temperatures. Thereby, the spin ordering changes into a conical structure. $ZnCr_2S_4$ shows two magnetic transitions at $T_{N1}=15$ K and $T_{N2}=8$ K that are accompanied by structural phase transitions. The crystal structure transforms from the cubic spinel-like (space group $Fd\bar{3}m$) at high temperatures in the paramagnetic state, via a tetragonally distorted intermediate phase (space group $I4_1/amd$) for $T_{N2}<T<T_{N1}$ into a low-temperature orthorhombic phase (space group $Imma$) for $T<T_{N2}$. The cooperative displacement of sulfur ions by exchange striction is the origin of these structural phase transitions. The low-temperature structure of $ZnCr_2S_4$ is identical to the orthorhombic structure of magnetite below the Verwey transition. When applying a magnetic field of 5 T the system shows an induced negative thermal expansion in the intermediate magnetic phase as observed in $ZnCr_2Se_4$.

I. INTRODUCTION

Chromium spinels of stoichiometry ACr_2X_4 ($X=O,S,Se$) are frustrated magnets. Frustration is distinguished by the fact that it is impossible to satisfy all pairwise interactions simultaneously. The chromium ions of the spinel structure form a network of corner-sharing tetrahedra known as the pyrochlore lattice. For nearest-neighbor antiferromagnetic (AFM) exchange, strong geometric frustration (GF) arises due to the triangular arrangement of the ions. Additional frustration may be present due to the competition between ferromagnetic (FM) and AFM interactions. The different exchange interactions critically depend on the Cr-Cr distance. At small Cr-Cr separation strong direct AFM exchange dominates. At larger distances, additional 90° FM Cr-X-Cr and more complex Cr-X-A-X-Cr superexchange paths contribute. Despite remarkable different exchange interactions reflected in paramagnetic Curie-Weiss temperatures varying from −400 to +200 K, chromium spinels generally reveal intricate AFM order below a Néel temperature in the range of 10–20 K. The broad range of magnetic exchange strength and magnetic ground states has recently been summarized in a corresponding phase diagram.[1]

The large degeneracy resulting from frustration may be lifted by any additional interaction which enters in a nonperturbative way. This is the origin for the large variety of fascinating ground states that become available for frustrated systems and that depend on the very details of the interactions involved (e.g., exchange, anisotropy, magnitude of the spin, etc.). Spin liquids,[2] spin-ice states,[3,4] clusters or loops of a finite number of spins,[5–7] heavy-fermion-like behavior,[8,9] as well as singlet formation[10] are typical examples of these exotic ground states. In particular, in chromium and vanadium oxide spinels magnetic frustration is lifted via a coupling between spin and lattice degrees of freedom,[1,11] resulting in a magnetic[12] or spin-driven[13] Jahn-Teller effect. This is a remarkable behavior since the $3d^3$ electronic configuration of Cr^{3+} ions corresponds to a half-filled lower t_{2g} triplet. Hence, a spin-only ion with almost spherical charge distribution and negligible spin-orbit coupling is expected. Structural distortions at low temperatures, induced by a gain in magnetic energy, are thus a novel kind of magnetoelastic coupling. For $ZnCr_2O_4$ and $CdCr_2O_4$, such a spin-lattice coupling has been discussed in terms of a spin-Peierls-type transition.[14–16]

However, a strong spin-lattice coupling may not necessarily involve static lattice distortions but may be purely dynamic in nature. The coupling of magnetic exchange interactions and long-range magnetic order to phonon modes has been put forward many years ago.[17–19] Recent *ab initio* calculations evidenced a magnetic-exchange-induced splitting of phonon modes decoupled from static lattice distortions.[20,21] These findings are in agreement with recent experimental infrared (IR) studies on the spin-phonon coupling of a large number of chromium spinels.[1]

$ZnCr_2S_4$ exhibits two subsequent AFM transitions at $T_{N1}=15$ K and $T_{N2}=8$ K, as evidenced by measurements of the magnetization, specific heat, thermal expansion, and IR

spectroscopy.[22] As outlined above, a strong spin-phonon coupling induces a significant splitting of phonon modes at T_{N1} and T_{N2}. The corresponding anomalies in the specific heat and thermal expansion can be suppressed by an external magnetic field, thus evidencing its magnetic origin.[22] The magnetic susceptibility of $ZnCr_2S_4$ reveals a paramagnetic Curie-Weiss temperature close to 0 K as a result of the competition between FM and AFM exchange interactions which are almost equal in strength, a situation termed bond frustration.[22]

$ZnCr_2Se_4$ orders in a complex AFM structure below T_N =21 K despite strong FM exchange reflected in a large positive value of the Curie-Weiss temperature θ_{CW}=115 K.[23] The magnetic phase transition is of first order, as evidenced by sharp anomalies in the specific heat and thermal expansion.[24] The magnetic phase transition can be suppressed by an external magnetic field. $ZnCr_2Se_4$ reveals negative thermal expansion (NTE) below 75 K down to T_N and extremely large magnetostriction.[24] The magnetic transition is accompanied by small structural distortions with a lowering of the symmetry from cubic $Fd\bar{3}m$ to tetragonal $I4_1/amd$ (Ref. [25]) or orthorhombic $Fddd$.[26] The magnetic origin of the structural distortions is most clearly evidenced in the phonon spectra of $ZnCr_2Se_4$. IR spectroscopy revealed a pronounced splitting of the IR-active phonon modes at T_N that can be completely suppressed by the application of an external magnetic field.[27]

Ferroelectricity has attracted a lot of interest, in particular when strongly coupled to magnetic properties in terms of multiferroic behavior. This phenomenon has been mainly observed in the perovskites $RMnO_3$ (R=rare earth) [28] and, more recently, in other materials.[29,30] It occurs in helical magnets where the spin spiral plane is perpendicular to the propagation vector. It has also been observed in the spinel $CoCr_2O_4$ with a conical spiral.[31] New studies have been made in order to explore multiferroic states in other kinds of helimagnets in which the magnetic propagation wave vector is perpendicular to spin spiral plane. However, according to the spin-current model,[32] or equivalently the inverse Dzyaloshinskii-Moriya interaction,[33,34] this structure by itself cannot produce ferroelectricity. In order to obtain an electric polarization in such compounds, an external magnetic field is needed to be applied unparallel to the propagation wavevector direction, as demonstrated recently for $ZnCr_2Se_4$.[35]

Although these systems have been extensively studied, this paper particularly reports on the coexistence of the diffuse magnetic scattering and NTE in $ZnCr_2Se_4$ at zero and applied magnetic fields, as well as in $ZnCr_2S_4$ in external magnetic field. In addition, clear structural transformations in $ZnCr_2S_4$ from cubic to tetragonal at T_{N1} and from tetragonal to orthorhombic at T_{N2} are documented.

The experimental results of the present paper are presented separately for $ZnCr_2Se_4$ (Sec. III) and $ZnCr_2S_4$ (Sec. IV). First, we report on extensive neutron powder diffraction (NPD) studies of $ZnCr_2Se_4$ in zero magnetic field from 2 to 300 K that revealed the existence of NTE. Moreover, the magnetic structure was determined without considering any structural distortions in order to simplify the analysis. Subsequently, we investigated the effect of an applied magnetic

field on the crystallographic and magnetic structures of $ZnCr_2Se_4$. In Sec. II, we present high-resolution synchrotron x-ray diffraction measurements of $ZnCr_2S_4$ that provide evidence for modifications of the crystal structure, accompanying the magnetic transitions, followed by neutron diffraction studies in zero field for obtaining the magnetic structure of the sulfide. Finally, we show results in external magnetic field evidencing field-induced NTE in the sulfide compound, similar to that observed in the selenide.

II. EXPERIMENTAL

Polycrystalline samples of $ZnCr_2S_4$ and $ZnCr_2Se_4$ were prepared by conventional solid-state synthesis from high-purity elements at 800 °C in evacuated quartz ampoules. To assure complete chemical reaction and to achieve single-phase material with good homogeneity, the sintering process was repeated several times with intermediate grinding and pressing of the material.

High-resolution NPD data were measured for both samples using the fine-resolution neutron powder diffractometer E9 located at the Berlin Neutron Scattering Center (BENSC) of the Helmholtz Center Berlin. The NPD data were measured in zero field and in an applied vertical magnetic field of 5 T as a function of temperature in the range of 2–300 K. The experiments were performed using neutron wavelength of either λ=1.797 Å or λ=2.4 Å with a resolution [full width at half maximum (FWHM)] of $\Delta d/d$ ～0.2%.[36] For $ZnCr_2S_4$ additional high-intensity NPD data were measured as a function of temperature on the E6 diffractometer (also at BESNC) with a wavelength of λ =2.4 Å. Both x-ray and neutron diffraction data were analyzed by the Rietveld method employing the FULLPROF suite of programs.[37]

The NPD data were modeled for all temperatures and fields employing the cubic spinel structure which is described by space group $Fd\bar{3}m$ with the Cr atoms at the Wyckoff position $16d$ (0.5,0.5,0.5) and the Zn ions at the Wyckoff position $8a$ (0.125,0.125,0.125). The Se and S atoms reside on Wyckoff position $32e$ (x,x,x) with x=0.259 4(1) for $ZnCr_2Se_4$ and x=0.258 3(1) for $ZnCr_2S_4$, respectively. Typical Caglioti resolution parameters that accounted for the angular dependence of the width of the Bragg reflections were refined from the Rietveld analysis to be U=0.0776°, V=−0.1337°, and W=0.1265°. For both compounds, magnetic scattering was observed below T_N and was simultaneously refined with the crystal structure within our Rietveld analysis. The corresponding magnetic models are described below.

High-resolution x-ray powder diffraction (XPD) data were measured from $ZnCr_2S_4$ at the beamline ID31 of the European Synchrotron Radiation Facility (ESRF, Grenoble).[38] The sample was placed in an aluminum container and mounted in a liquid-helium-cooled cryostat. The measurements were performed in a temperature range of 2–40 K. An incident wavelength of λ=0.39950 Å in combination with a large range of the scattering angle −5.964° $<2\theta<$67.968° allowed measurements up to 17.8 A^{-1} of the scattering vector Q=$4\pi \sin(\theta)/\lambda$. Three different phases
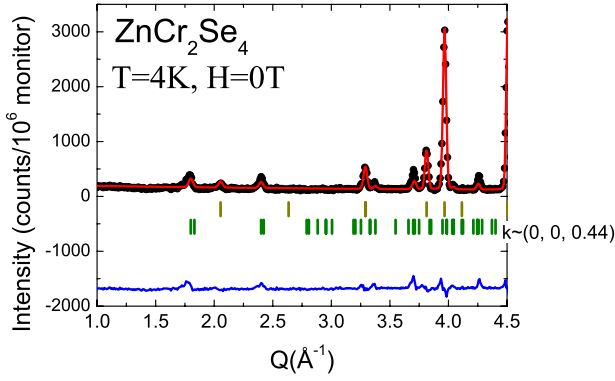
FIG. 1. (Color online) Rietveld refinement of the NPD date measured from $ZnCr_2Se_4$ at 4 K in zero field using $\lambda = 1.797$ Å. The black points represent the experimental data while the red and blue lines correspond to the refinement and the difference between calculated and experimentally observed intensities, respectively. The upper row of tick marks shows the calculated positions of nuclear Bragg reflections (dark yellow) and the lower row indicates the calculated position of magnetic reflections (dark green) with $k \sim (0,0,0.44)$ [Note that $q = 4\pi \sin(2\theta/2)/\lambda$].

have been refined simultaneously: the main phase $ZnCr_2S_4$, aluminum scattering arising from the sample holder and cryostat, and Cr_2S_3 as a residual of the sample preparation procedure. The refinements indicate a mean volume fraction of 2.3% of the spurious phase close to sensitivity limit of conventional powder diffraction. Apart from instrumental parameters (peak shape and resolution parameters), an overall scale factor, the lattice constants, the sulfur position, and isotropic temperature factor for each atomic species were refined.

III. NEUTRON POWDER DIFFRACTION OF ZnCr₂Se₄

A. Zero-field NPD measurements of ZnCr₂Se₄

Within the experimental accuracy, the NPD data of $ZnCr_2Se_4$ are consistent with the well-known spinel $Fd\bar{3}m$ crystal structure at all temperatures and fields. In zero field, several magnetic reflections are detected at low diffraction angles below $T_N = 21$ K, as shown in Fig. 1. These magnetic reflections can be indexed by a propagation vector $k \sim (0,0,\delta)$ with $\delta \sim 0.44$. It is reported that this magnetic transition is accompanied by a structural transition to an orthorhombic space group $Fddd$[24,26] with a small orthorhombic distortion of $c/a = 0.9999$ at 20 K and $a \cong b$.[24–26] Examination of the present NPD data revealed no evidence for such a transition as the size of this distortion is below the detection limit set by the Q resolution of our instrument. For the analysis of the NPD data we therefore continued to use the cubic spinel structure also for the low-temperature data below T_N.

The magnetic scattering below T_N was modeled using the spherical harmonics approach and considering four Cr atoms in the primitive unit cell stacked along the c axis as reported in the literature.[26,39] We found that the data were consistent with a model where Cr spins form ferromagnetic layers that
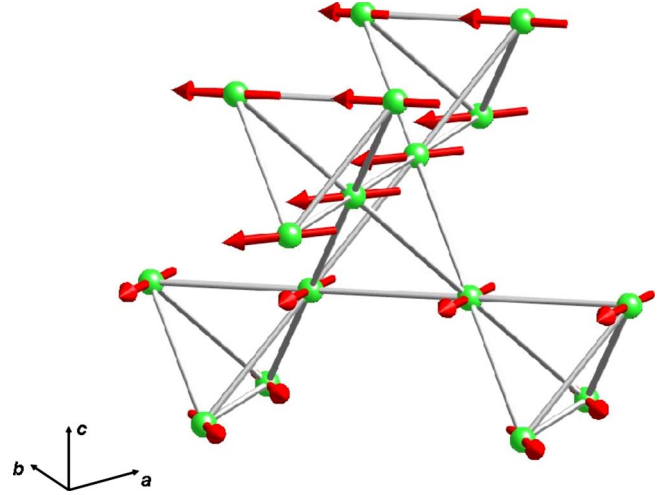

FIG. 2. (Color online) Schematic representation of the magnetic structure of $ZnCr_2Se_4$. For clarity only the Cr atoms are displayed.

are coupled antiferromagnetically along the c axis. The ordering along the c axis is incommensurate (IC) and naturally leads to a helical magnetic structure propagating along the unique c axis as illustrated in Fig. 2. Rietveld refinement of the 2 K data results in a screw angle of 42° and a magnetic moment of the Cr atoms of $1.90(2)\mu_B$, somewhat higher than the value of $1.54\mu_B$ reported in Ref. 39. On warming, we find a change in the incommensurability δ toward lower values consistent with previous reports.[39,40] The screw angle and the Cr moment varies smoothly with increasing temperature, as shown in Fig. 3, reaching final values of 39° and $1.4(2)\mu_B$ at $T_N = 21$ K, respectively. The jump of the ordered magnetic moment at T_N indicates a first-order phase transition, in agreement with heat-capacity and thermal expansion measurements.[24] The first-order nature of the magnetic transition is probably related to the accompanying structural modifications.

We now turn our attention to the structural parameters determined by Rietveld analysis of the NPD data above T_N. We find that the cubic lattice constant a shows a positive
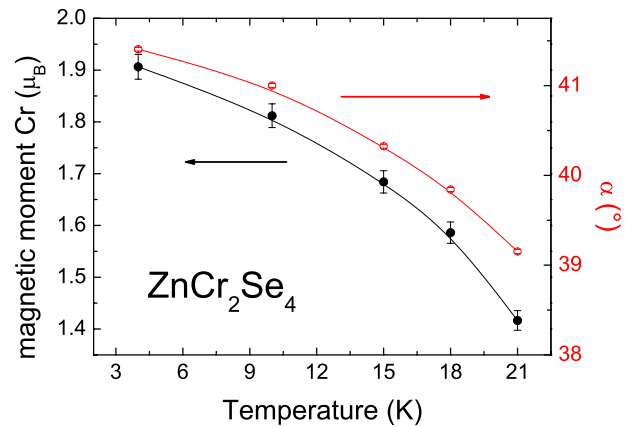

FIG. 3. (Color online) Ordered magnetic moment of Cr atoms (black, left side axis) and screw angle α (red, right side axis) vs temperature in $ZnCr_2Se_4$ determined from Rietveld analysis of the NPD data. Full lines are to guide the eyes.
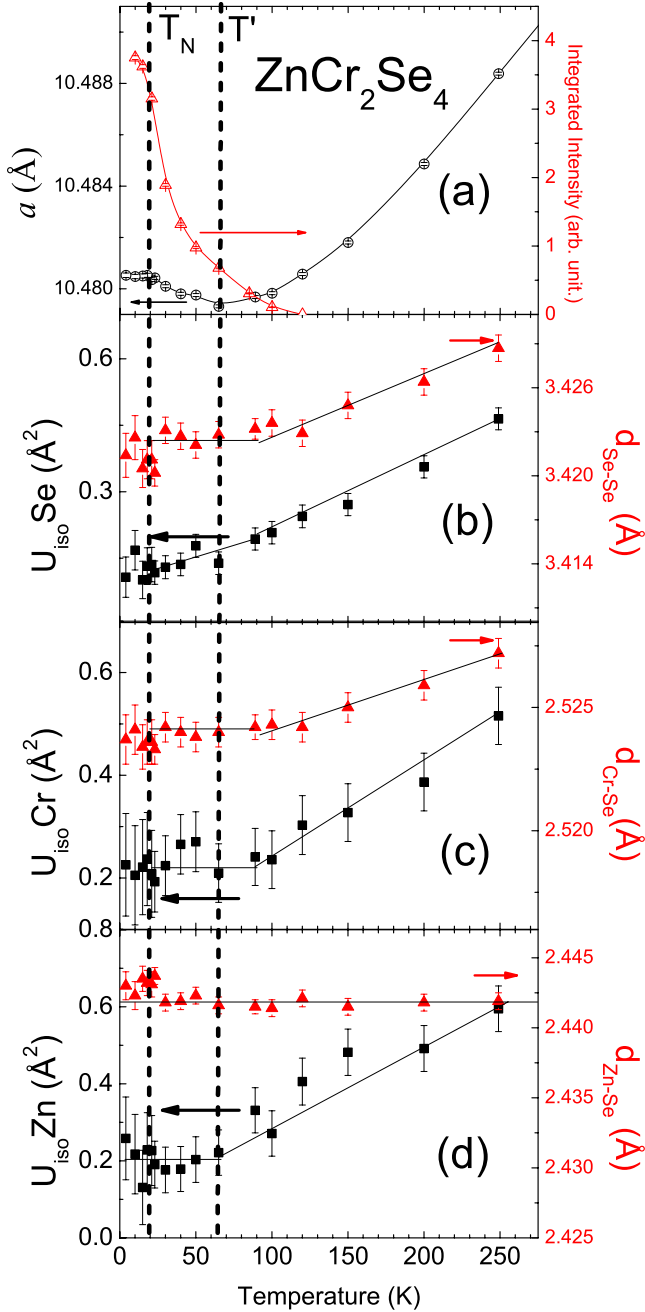
FIG. 4. (Color online) (a) Temperature dependence of the lattice constant a of the integrated diffuse magnetic intensity around the first magnetic reflection. The Se-Se, Cr-Se, and Zn-Se bond lengths of the function of temperature are shown in panels (b) and (c), respectively, together with U_{iso} values of Se, Cr, and Zn in the same panel, respectively. The lines are drawn to guide the eyes.

thermal expansion between 79 and 300 K [Fig. 4(a)]. This normal behavior of the crystal lattice is also reflected in the Cr-Se and Cr-Cr bond lengths, as well as in the isotropic atomic displacement parameters (U_{iso}) of Cr and of Zn atoms [see Figs. 4(b)–4(d)], all of which decrease linearly over this region in temperature. For the Zn-Se bond length we find an unusual behavior: it remains essentially temperature invariant over the entire temperature range examined, showing a slight increase below T_N. The latter feature may be indicative
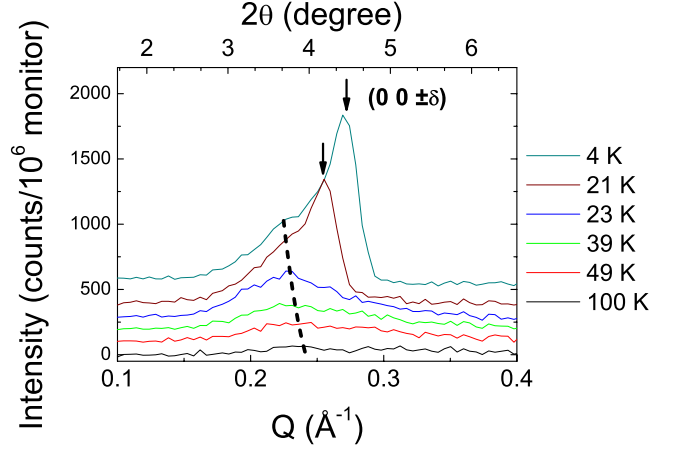

FIG. 5. (Color online) The magnetic diffuse scattering at 100, 49, 39, and 23 K from ZnCr$_2$Se$_4$ developing into the magnetic $(0, 0, \pm \delta)$ reflection at 21 and 4 K below T_N. The dashed line is a guide to the eyes to show the evolution of the magnetic diffuse scattering. The arrows show the positions of the magnetic peaks at 21 and 4 K. The scans are plotted with an offset of 100 counts per 10^6 monitors.

of an orthorhombic distortion below T_N, as reported elsewhere.[26] On further cooling below $T' \sim 68$ K the cubic lattice constant exhibits NTE until T_N. Below T' we also find that the U_{iso} value of the Cr atom, as well as the Cr-Se bond length, becomes temperature independent, further suggesting an anomalous structural behavior. We did not detect a structural phase transition at T' consistent with previous structural investigations that report cubic symmetry for $T > T_N$. This suggests that the observed structural behavior over the temperature region $T_N < T < T'$ may originate from local symmetry breaking only. Below T_N and within the resolution of our instrument we find an essentially constant value of the lattice constant a. However, we believe that the refined structural parameters of the NPD data reflect the average of a slightly orthorhombically distorted structure, and our measurements are insensitive to this small orthorhombic distortion.

The onset of the NTE may be closely related to the behavior of the Cr spins. Specific-heat and magnetization measurements[24] suggest strong spin fluctuations below T'. Indeed, broad diffuse scattering contributions centered on the $(0, 0, \delta)$ magnetic reflections are observed for temperatures as high as 100 K. As illustrated in Fig. 5, this diffuse scattering becomes narrower on cooling. Below $T_N = 21$ K, a sharp peak appears that is related to the helical magnetic structure. The broad peak corresponding to magnetic fluctuations coexists with the magnetic Bragg reflection within the long-range ordered ground state. This behavior is reminiscent of the complex magnetic ordering process of the A-site spinel MnSc$_2$S$_4$[41] that was interpreted in terms of a spiral spin liquid.[42] The asymmetry of the broad peak is due to the FM correlations within the a-b planes. In Fig. 4(a), we plot the integrated intensity of the magnetic diffuse scattering around the $(0, 0, \delta)$ reflection as a function of temperature. This intensity appears above T' and rapidly increases as T_N is approached. The simplest plausible explanation of this

scattering is that it arises from small antiferromagnetic clusters with an average size of $d \approx 53$ Å at $T \approx 23$ K as given by the width (FWHM) of the diffuse magnetic scattering. This observation is suggestive for a magnetoelastic coupling above T_N within the spin fluctuation regime that leads to NTE of the lattice below T'.

B. High-field NPD measurements of ZnCr₂Se₄

We investigated the effect of a magnetic field on the crystal and magnetic structures of ZnCr₂Se₄ by measuring NPD data as a function of temperature in a vertical magnetic field of 5 T. In this case, magnetic scattering was observed only below 9 K indicating a suppression of T_N as compared to the zero-field measurements. Moreover, significant field-induced changes in the magnetic intensities are observed. These changes are summarized in Fig. 6. At 19 K and 5 T we find a strong enhancement of the nuclear $(1,1,1)$ Bragg reflection compared to the zero-field data, while the helical $(1, 1, 1 \pm \delta)$ reflections are absent [Fig. 6(a)]. However, at the same temperature we find broad diffuse intensity around the $(0, 0, \delta)$ reflection [see Fig. 6(d)] indicative of magnetic short-range helical correlations (the correlation length is ≈ 42 Å at 20 K). On further cooling, these short-ranged helical correlations developed into sharp magnetic Bragg reflections below 9 K [see Figs. 6(b) and 6(c)] indicating that the 5 T ground state is an induced ferromagnet with a weak residual AFM component (with a correlation length at 4 K of ≈ 115 Å).

We now turn to the crystal structure of ZnCr₂Se₄ in a magnetic field of 5 T. The most interesting aspect is the persistence of a NTE from 20 K (the highest temperature for an applied magnetic field of 5 T) to 2 K. In Fig. 7 we compare the temperature dependence of the cubic a axis for both zero-field and 5 T measurements in terms of the normalized lattice constant $[a(T) - a(2 \text{ K})]/a(2 \text{ K})$. The increase in the (average) lattice constant appears to track the intensity of the AFM helical Bragg reflections, similar to that observed for zero-field data [see Fig. 4(a)].

IV. CRYSTAL AND MAGNETIC STRUCTURES OF ZnCr₂S₄

A. Synchrotron x-ray diffraction

We now turn to the crystal structure of ZnCr₂S₄. In the upper panel of Fig. 8 we show an example of the XPD pattern collected from our ZnCr₂S₄ sample. The sample was of excellent quality as sharp resolution-limited diffraction peaks could be observed up to extremely high Q values. Due to the extraordinarily high resolution, Bragg reflections appear as vertical lines on this scale. The inset shows a strongly expanded view around $2\theta \approx 4°$ corresponding to the first reflection of the diffraction pattern. Additionally to the dominating (101) reflection of ZnCr₂S₄, now a weak intensity of residual Cr₂S₃ appears. A magnification around 29° scattering angle evidences the different peak splitting due to the structural phase transitions which are discussed below.

ZnCr₂S₄ passes through a first magnetic transition at $T_{N1} = 15$ K[22,43] which is accompanied by a structural phase transition. For $T > 15$ K in the paramagnetic regime,

ZnCr₂S₄ crystallizes in the normal cubic spinel structure described by space group $Fd\bar{3}m$ in which the atoms Zn, Cr, and S are located at the Wyckoff positions $8a$, $16d$, and $32e$, respectively. At 14 K, the crystal structure changes to tetragonal symmetry of space group $I4_1/amd$ (No. 141, origin choice 2) with half the unit-cell volume $V_{\text{tetragonal}} = a/\sqrt{2} \times a/\sqrt{2} \times a$ of the cubic cell. The tetragonal crystal structure is observed in the temperature range between the first and the second magnetic transitions $T_{N1} > T > T_{N2}$ (7–14 K). In this structure, the atoms Zn, Cr, and S are found at the Wyckoff positions $4a$ $(0,3/4,1/8)$, $8d$ $(0,0,1/2)$, and $16h$ $(0,y,z)$, respectively. Below 7 K, a further structural phase transition into orthorhombic symmetry described by space group $Imma$ takes place. Apart from the metric of the unit cell, the only structural parameters are the sulfur positions since the Zn and Cr ions are always located at special high-symmetry sites. For a given crystal structure, the sulfur positional parameters remain virtually constant without any significant temperature dependence. The same holds true for the isotropic temperature factors of all three ion types that remain almost constant with some scattering around $B_{\text{iso}} \approx 0.2$ (Å²). Only in the vicinity of T_{N2} (specifically for $T = 5$, 7, and 8 K) all temperature factors show enhanced values of about 0.4 Å².

The results of the structure refinements are detailed in Table I at $T = 2$ K (orthorhombic phase), $T = 9$ K (within the tetragonal phase), and 17 K (cubic phase). Figure 9 shows the temperature dependence of the lattice constants of ZnCr₂S₄. For a direct comparison, the lattice parameters a (and b) of the tetragonal (orthorhombic) phases have been normalized by multiplication with $\sqrt{2}$. Evidently, the magnetic transitions are directly followed by changes in the crystal structure.

B. Zero-field NPD measurements of ZnCr₂S₄

The two antiferromagnetic transitions of ZnCr₂S₄ at $T_{N1} = 15$ K and $T_{N2} = 8$ K are also reflected in the temperature-dependent NPD data shown in Fig. 10. Below T_{N1}, at 14K, we observe 12 magnetic peaks at low Q, which all can be indexed by the propagation vector $k_1 \sim (0, 0, \delta)$ with $\delta = 0.787(1)$. This ordering is very similar to that we found for the ZnCr₂Se₄ compound.[40,43] Here, our NPD data can be modeled using the same FM ordering in (001) planes with a screw angle between planes of $70.8(1)°$ at 14 K and a Cr magnetic moment of $1.23(3)\mu_B$, similar to the results of Ref. 43.

Below T_{N2} the ordering of Cr spins is more complex. On cooling, the intensity of the k_1 reflections decreases and below 8 K other commensurate reflections appear (Fig. 10) with propagation vectors $k_2 = (0.5, 0.5, 0)$ and $k_3 = (1.0, 0.5, 0)$. Indeed the same behavior in the magnetic structure of ZrCr₂S₄ was noted in previous work.[43]

Modeling the magnetic structure of ZrCr₂S₄ below T_{N2} is especially challenging considering that the symmetry of the k_2 and k_3 magnetic wave vectors in general is not exclusively orthogonal to k_1. This is certainly the case for k_2; however, k_3 can describe a collinear magnetic structure with ferromagnetic planes perpendicular to k_3 which are arranged as a +
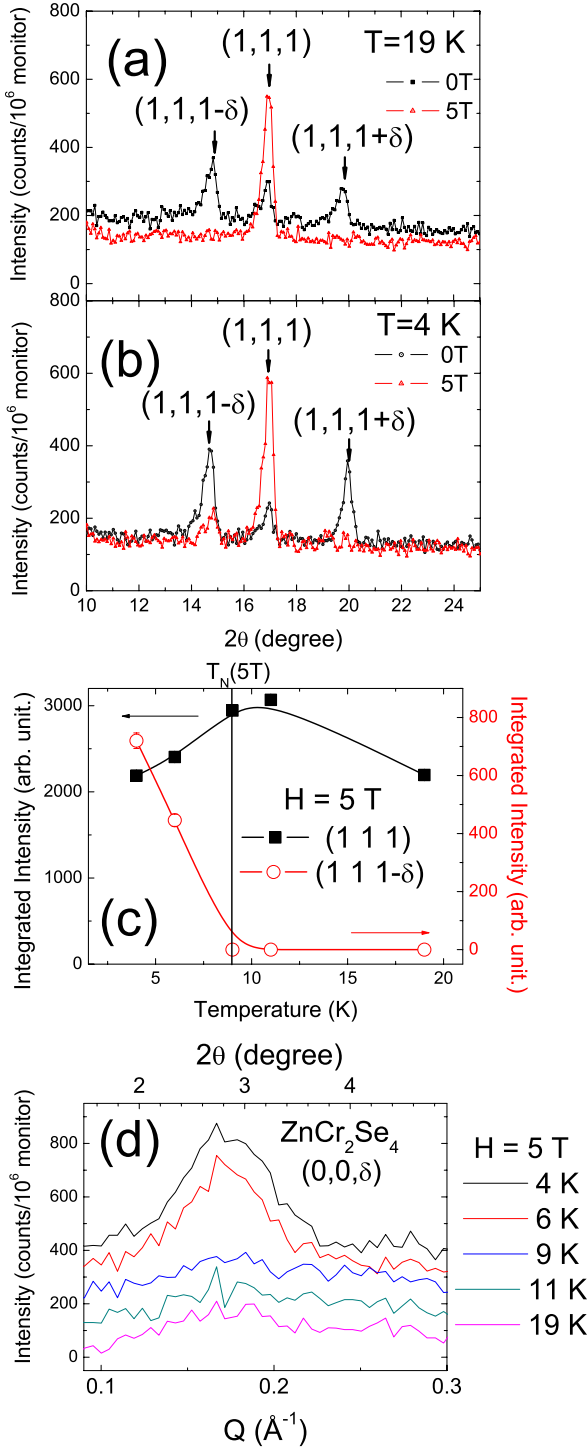
FIG. 6. (Color online) Low-angle portion of the neutron diffraction pattern of $ZnCr_2Se_4$ around the (1,1,1) reflection obtained in zero field (black line) and in an applied magnetic field of 5 T (red) at (a) 19 K and (b) 4 K. In panel (c), the temperature dependence of the integrated intensities of the nuclear Bragg reflection (1,1,1) (black squares) and the corresponding magnetic satellite $(1,1,1-\delta)$ (red circles) are shown. The vertical line indicates the magnetic ordering temperature in a field of 5 T, where as the dashed lines serve to guide the eyes. Panel (d) shows the magnetic $(0,0,\pm\delta)$ Bragg reflection in a magnetic field of 5 T for various temperatures (the scans are plotted with an offset of 100 counts per 10^6 monitors). Measurements were performed on E9 with $\lambda = 1.797$ Å.
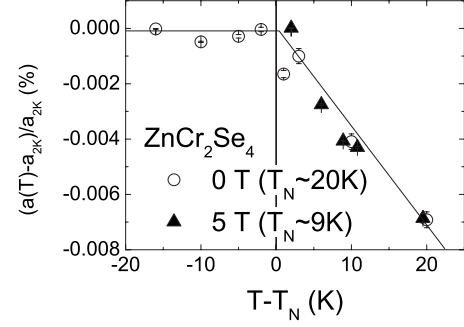

FIG. 7. Normalized lattice parameter a of $ZnCr_2Se_4$ versus reduced temperature $T-T_N$ at 0 and 5 T, respectively. Lines are drawn to guide the eyes.

+−− sequence along the propagation vector and orthogonal to k_1. Hamedoun *et al.*[43] argued that such, apparently complicated, magnetic structure reflects the chemical complexity of the samples. The variation of the magnetic components for the three different wave vectors in different samples prepared under different partial pressure of S leads to the conclusion
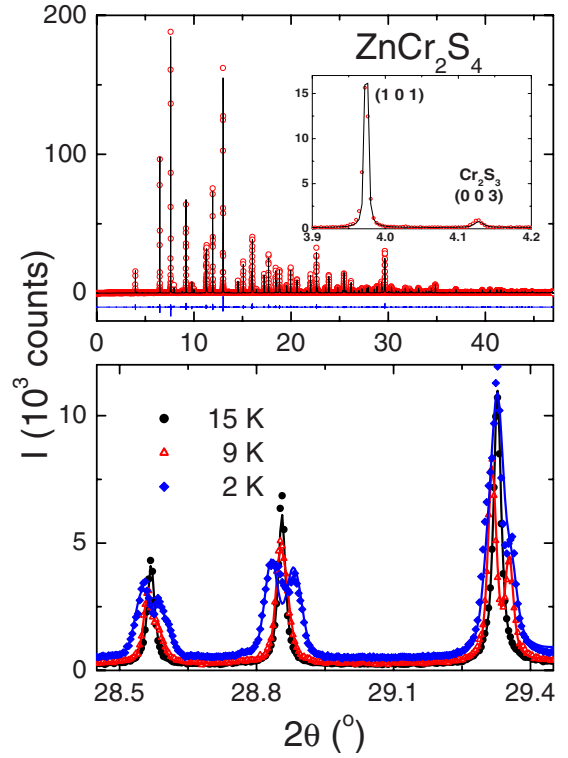

FIG. 8. (Color online) X-ray powder diffraction pattern of $ZnCr_2S_4$ using $\lambda = 0.399\,50$ Å. In the upper part, observed (red circles) and calculated (black line) intensities and their difference (blue line at the bottom) are shown for $T=9$ K. The inset shows the first reflections (1,0,1) of $ZnCr_2S_4$ and (0,0,3) of Cr_2S_3 around $2\theta \approx 4°$ to illustrate the weak contribution of the spurious phase with a respective volume fraction of about 2%. The lower frame shows the diffraction pattern of $ZnCr_2S_4$ for various temperatures $T=2$, 9, and 15 K in a small angular range to evidence the corresponding peak splitting across the two structural phase transitions as described in the text. Again, symbols refer to observed and lines to calculated profiles, respectively.

TABLE I. Crystallographic structure of ZnCr$_2$S$_4$ as obtained from Rietveld refinements of high-resolution x-ray powder diffraction for $T=2$, 9, and 17 K, respectively. Listed are the lattice constants a, b, and c, the sulfur positional parameters in fractional coordinates, the isotropic temperature factors, and the residuals of the refinement R_{Bragg} and R_F. Only the low-temperature *Imma* phase has two different sulfur sites.

ZnCr$_2$S$_4$	*Imma*	I_1/amd	$Fd\bar{3}m$
T (K)	2	9	17
a (Å)	7.04679(5)	7.06116(2)	9.98152(2)
b (Å)	7.06743(5)		
c (Å)	9.98328(8)	9.97137(4)	
x (S1)	0	0	0.25972(3)
x (S2)	0.26136(9)		
y (S1)	0.52253(18)	0.019567(13)	0.25970(3)
y (S2)	0.25		
z (S1)	0.26136(9)	0.25955(11)	0.25970(3)
z (S1)	−0.01136(9)		
B_{Zn} (Å^2)	0.131(13)	0.203(8)	0.127(6)
B_{Cr} (Å^2)	0.189(39)	0.200(9)	0.126(6)
B_S (Å^2)	0.184(17)	0.221(9)	0.135(7)
R_{Bragg} (%)	4.36	3.48	3.69
R_F (%)	4.72	3.52	3.89

that the apparent complexity in the magnetic ordering arises from S vacancies,[43] with the differences between powder and single-crystal samples being especially pronounced. Such behavior is proposed to arise due to the sensitivity of the exchange parameters to the Cr-Cr distance which is in turn are modulated by S vacancies. A calculation of the free energy between the possible magnetic structures represented by k_1 and k_2 differs by only ~0.1 K[43] further highlighting the virtual degeneracy of these states. Application of the same magnetic model used by Hamedoun *et al.*[43] to our NPD data measured at 2 K yielded similar results. Here we deduce $m_1=1.13(2)$, $m_2=1.18(2)$, and $m_3=0.69(4)\mu_B$ per Cr, com-
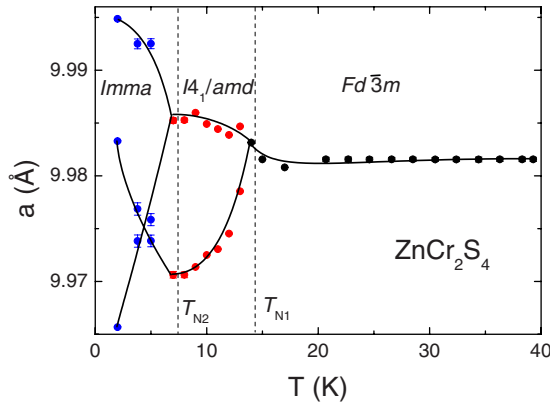

FIG. 9. (Color online) Temperature-dependent normalized lattice constants of ZnCr$_2$S$_4$. The magnetic transition temperatures and the space groups of the different structures are indicated. The solid lines are to guide the eyes.
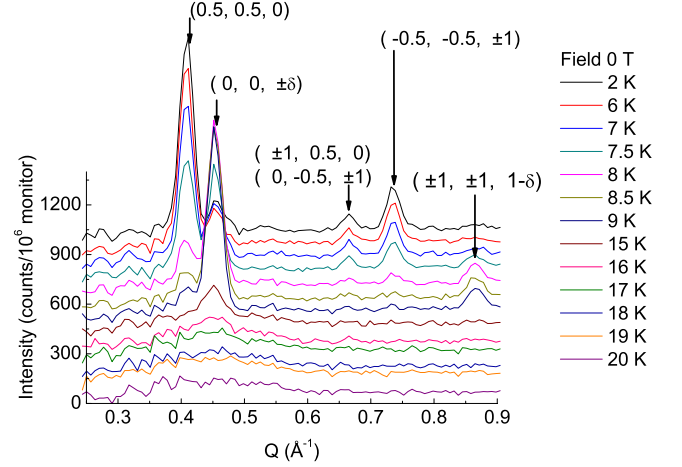

FIG. 10. (Color online) Temperature dependence of the first magnetic peaks of ZnCr$_2$S$_4$ with propagation vectors k_1 $=(0,0,0.787)$, $k_2=(1,0.5,0)$, and $k_3=(0.5,0.5,0)$. Measurements were performed on E6 with $\lambda=2.446$ Å. The scans are plotted with an offset of 70 counts per 10^6 monitors.

pared to 1.23, 1.53, and $0.85\mu_B$ per Cr, respectively.

If indeed the magnitude of these magnetic moments is dependent on S inhomogeneities it is peculiar that our results would be so similar to those of reported previously. To test further possible solutions to the magnetic structure of ZrCr$_2$S$_4$ below T_{N2} assuming a single magnetic phase, we performed symmetry analysis and phenomenological fits to the NPD data on the basis of the low-temperature orthorhombic phase (Fig. 11). Our working assumption was to test if the magnetic scattering described by k_2 and k_3 can arise from components of the Cr moment that are perpendicular to the ferromagnetic planes described by the k_1 wave vector.

For k_2, the symmetry analysis presents the possibility of components of the Cr moment that are parallel to the c axis (i.e., orthogonal to Cr moments described by k_1). Poor fits to
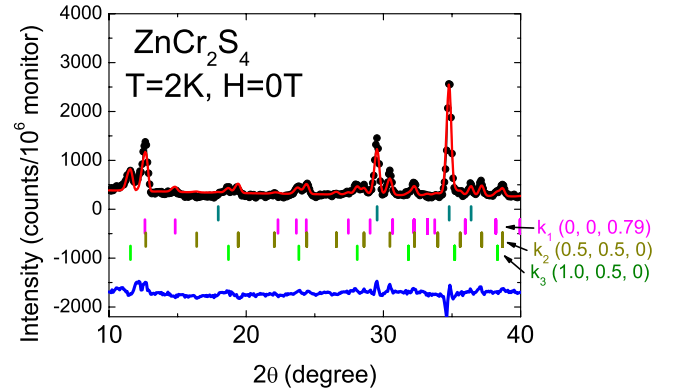

FIG. 11. (Color online) Rietveld analysis of NPD data measured from ZnCr$_2$S$_4$. The black points represent the experimental data while the red and blue lines represent the model and the difference between the experimental data and the model, respectively. The tick marks show the expected positions of nuclear Bragg reflections and magnetic reflections from the three magnetic orderings described by propagation vectors k_1, k_2, and k_3. Here we have considered that the three propagation vectors are in three spatially separated magnetic phases.
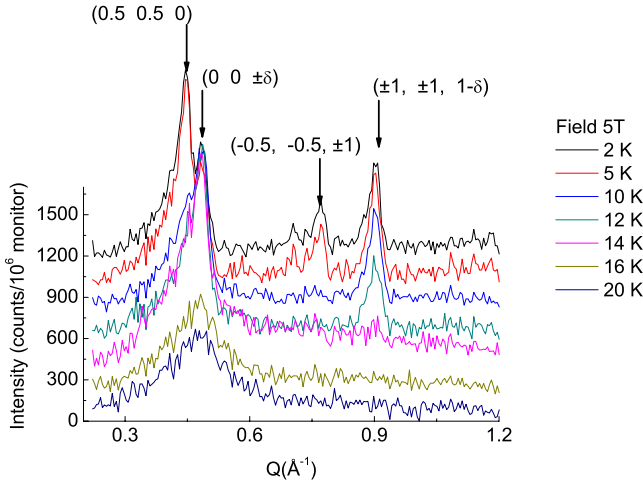
FIG. 12. (Color online) Low-angle magnetic reflections of $ZnCr_2S_4$ in an applied magnetic field of 5 T for various temperatures. NPD data were measured on E9 with $\lambda = 1.797$ Å. The scans are plotted with an offset of 70 counts per 10^6 monitors.

the NPD data were obtained for k_2 Bragg peaks when constraining the Cr moment to be parallel to the c axis. Better results, however, were obtained when the Cr moments were allowed to have components in the [110] plane, clearly demonstrating that k_1 and k_2 spins are not orthogonal and therefore cannot arise from the same chemical phase. A similar analysis for the k_3 propagation vector shows that the magnetic intensity of these Bragg reflections can be modeled only with Cr spin components that are parallel to the c axis, indicating a compatibility between the k_1 and k_3 wave vectors. Assuming such a configuration and analyzing the NPD data with two magnetic phases ($k_1 + k_3$ and k_2), we obtained $m_{1+3} = 1.63(2)$ and $m_2 = 2.16(2)$. However, we note that a thorough search of the NPD data could not identify Bragg reflection with $k = k_1 + k_2 = (1, 0.5, \delta)$, suggesting again that k_1 and k_3 likely do not arise from the same chemical phase. To make further progress in describing the true magnetic ground state of $ZrCr_2S_4$, single-crystal measurements from stoichiometric samples are required, an endeavor beyond the scope of the present work.

C. High-field NPD measurements of $ZnCr_2S_4$

Given the degeneracy between the different magnetic orderings in $ZnCr_2S_4$, the application of a magnetic field offers the possibility of energetically favoring one of these states. Indeed, NPD as a function of temperature in an applied field of 5T indicates that the helical magnetic structure (k_1) is preferred at the expense of the two commensurate orderings (k_2 and k_3). This behavior is evidenced in Fig. 12. At 20 K and 5 T, the magnetic scattering appears as a broad diffuse reflection indicative of AFM fluctuations. On cooling, this scattering becomes sharper indicative of a long-range helical magnetic ordering below $T_N(5 \text{ T}) = 14$ K. The magnetic structure at 10 K, described by the incommensurate wave vector $k_1 = (0, 0, 0.78(1))$, gives a helical angle for the Cr spins of $70.2(9)°$. On further cooling below 5 K, the commensurate reflections with propagation vectors k_2 and k_3 ap-
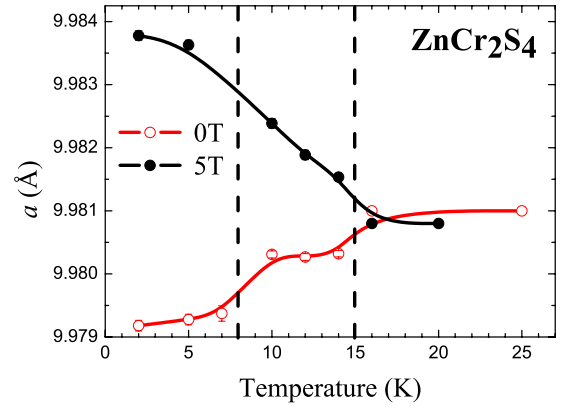

FIG. 13. (Color online) Comparison of the temperature dependence of the lattice parameter a for a magnetic field of 5 T (black line and full circles) and in zero field (red line and open circles). Lines are drawn to guide the eyes.

pear while the intensity of the commensurate reflections is significantly suppressed compared to the zero-field data. Thus a 5 T field leads to a ground state that is similar to that of $ZnCr_2Se_4$ at zero field, albeit with additional small commensurate components k_2 and k_3.

The dominant helical spin ordering at 5 T is also evidenced in the thermal expansion. In Fig. 13 the temperature dependence of the average cubic lattice constant in zero field and 5 T is shown. An overall positive thermal expansion in zero field is observed while the 5 T data reveal a NTE coinciding with the onset of helical ordering. This behavior is reminiscent of the zero-field measurements of the $ZnCr_2Se_4$ samples. It may suggest that the helical spin ordering induces frustration onto the lattice that leads to anomalous thermal expansion, as well as anomalies in the phonon spectra.[24]

V. DISCUSSION

Spin-lattice coupling has turned out to be an efficient way to lift frustration. Therefore, the magnetic structure and structural distortions in chromium spinels are strongly correlated. $ZnCr_2O_4$ exhibits a small Cr-Cr distance and, consequently, a strong direct AFM exchange as reflected in a large negative Curie-Weiss temperature. Below $T_N = 12.5$ K it orders antiferromagnetically in a commensurate but complex multi-**k** structure whose details depend on sample preparation conditions.[44] The accompanying structural phase transition is characterized by a contraction of the c axis and structural superlattice peaks of type $(1/2, 1/2, 1/2)$ corresponding to the tetragonal space group $I\bar{4}m2$.[44] $CdCr_2O_4$ has somewhat larger Cr-Cr distance but still dominating AFM exchange. It reveals an incommensurate spin structure with propagation vector $\mathbf{k} = (0, \approx 0.09, 1)$ and an elongated c axis within tetragonal symmetry of space group $I4_1/amd$. On the other hand, $ZnCr_2Se_4$ with the largest Cr-Cr separation has strong FM exchange evidenced by a large positive Curie-Weiss temperature of $\theta_{CW} = 115$ K. A structural phase transition takes place at $T_N = 21$ K from cubic $Fd\bar{3}m$ to orthorhombic $Fddd$ symmetry with a contraction of the c axis.[26] $ZnCr_2Se_4$ reveals an incommensurate helical spin structure with FM

layers and AFM coupling along the orthorhombic c axis of rotation. For $ZnCr_2S_4$, both FM and AFM interactions are almost equal in strength leading to a Curie-Weiss temperature close to zero.[1] The subtle balance between two competing interactions is easily disturbed and therefore a strong sensitivity of the magnetic properties on slight structural distortions is expected. Neutron diffraction revealed the onset of a helical spin structure at T_{N1}. Below 12 K, the helical structure transforms into two collinear structures with wave vectors $[1/2, 1/2, 0]$ and $[1, 1/2, 0]$.[43] At low temperatures, a coexistence of all three phases was suggested. Along the magnetic structure determination, an upper limit of $1 - c/a$ < 0.002 has been reported for any static structural distortions.[43] The magnetic structure of $ZnCr_2S_4$ below T_{N1} $=15$ K is similar to that of the Se homolog, formed by dominating FM interactions leading to FM layers. To account for the additional AFM exchange, a helix is formed with a rotation axis perpendicular to $[110]$. Upon further cooling, the relative weight of the AFM exchange increases and the helix transforms into commensurate AFM structures reminiscent of $ZnCr_2O_4$ with identical propagation vectors. A phase coexistence has been proposed based on the fact that significant differences in the diffraction intensities between powder and single-crystalline samples were observed.[43] In view of the sensitivity of the magnetic properties on sample preparation conditions, e.g., vacancies, such a conclusion has to be considered with care. Our present high-resolution x-ray diffraction study revealed structural phase transitions from cubic $Fd\bar{3}m$ to tetragonal $I4_1/amd$ symmetry just below T_{N1} and from tetragonal $I4_1/amd$ to orthorhombic $Imma$, just below T_{N2}, but no anomalous behavior around 12 K. For each temperature region, a single phase of $ZnCr_2S_4$ was sufficient to account for the measured diffraction pattern. It is interesting to note that the orthorhombic low-temperature structure of $ZnCr_2S_4$ is identical to that of magnetite below the Verwey transition with mutually perpendicular rows of ferric and ferrous ions along the $[110]$ directions.[45] A corresponding scenario in case of $ZnCr_2S_4$ would be that below $T_{N2}=8$ K, the helix of FM spin chains adopts a phase of $\pi/2$ leading to a spin arrangement of perpendicular FM spin chains along $[110]$. This would correspond to a magnetic analog of the charge order process in Fe_3O_4. Regardless other measure-

ments on magnetic field in $ZnCr_2S_4$ clearly demonstrate the greater stability of the helical ordering compared to the commensurate k_2 and k_3 orderings.

The formation of ferromagnetic layers in $ZnCr_2Se_4$ evidenced by the magnetic fluctuations below 80 K, as shown in Fig. 5 at 0 T, induces frustration in the lattice parameter. One can argue that such behavior may be related to the observation of a NTE. In an applied magnetic field, the helical spin structure of $ZnCr_2Se_4$ becomes suppressed on increasing FM interactions, moving down the magnetic transition temperature and the temperature range of NTE. On the other hand, in case of $ZnCr_2S_4$, the magnetic field starts to break the delicate balance between AFM and FM interactions. An external magnetic field amplifies the FM interactions and induces a NTE behavior. $ZnCr_2S_4$ differs from the selenide compound as the helical spin structure is not suppressed in an applied magnetic field.

VI. CONCLUSION

In this paper we have presented a comparison of two closely related spinel compounds $ZnCr_2Se_4$ and $ZnCr_2S_4$. They reveal different magnetic structures originating from the subtle interplay between frustrated FM and AFM exchange interactions. In the selenide compound, we relate the evolution of incommensurate helical magnetic correlations and NTE as a consequence of magnetic frustration. The structural effects by an applied magnetic field can be accounted for accordingly by enhancing the FM component with respect to the AFM exchange.

The thio-spinel $ZnCr_2S_4$ exhibits two magnetic transitions accompanied by structural transformations. External magnetic field induces NTE below the first magnetic transition temperature and further suppresses the commensurate magnetic structural components in the second low-temperature magnetic phase of $ZnCr_2S_4$.

[1] T. Rudolf, Ch. Kant, F. Mayr, J. Hemberger, V. Tsurkan, and A. Loidl, New J. Phys. **9**, 76 (2007).

[2] B. Canals and C. Lacroix, Phys. Rev. Lett. **80**, 2933 (1998).

[3] A. P. Ramirez, A. Hayashi, R. J. Cava, R. Siddhartan, and B. S. Shastry, Nature (London) **399**, 333 (1999).

[4] S. P. Bramwell and M. J. P. Gringas, Science **294**, 1495 (2001).

[5] A. J. Garcia-Adeva and D. L. Huber, Phys. Rev. Lett. **85**, 4598 (2000).

[6] P. G. Radaelli, Y. Horibe, M. J. Gutmann, H. Ishibashi, C. H. Chen, R. M. Ibberson, Y. Koyama, Y.-S. Hor, V. Kiryukhin, and S.-W. Cheong, Nature (London) **416**, 155 (2002).

[7] S.-H. Lee, C. Broholm, W. Ratcliff, G. Gasparovic, Q. Huang, T. H. Kim, and S.-W. Cheong, Nature (London) **418**, 856 (2002).

[8] S. Kondo, D. C. Johnston, C. A. Swenson, F. Borsa, A. V. Mahajan, L. L. Miller, T. Gu, A. I. Goldman, M. B. Maple, D. A. Gajewski, E. J. Freeman, N. R. Dilley, R. P. Dickey, J. Merrin, K. Kojima, G. M. Luke, Y. J. Uemura, O. Chmaissem, and J. D. Jorgensen, Phys. Rev. Lett. **78**, 3729 (1997).

[9] A. Krimmel, A. Loidl, M. Klemm, S. Horn, and H. Schober, Phys. Rev. Lett. **82**, 2919 (1999).

[10] E. Berg, E. Altman, and A. Auerbach, Phys. Rev. Lett. **90**, 147204 (2003).

[11] M. Reehuis, A. Krimmel, N. Büttgen, A. Loidl, and A. Prokofiev, Eur. Phys. J. B **35**, 311 (2003).

[12] O. Tchernyshyov, R. Moessner, and S. L. Sondhi, Phys. Rev. Lett. **88**, 067203 (2002).

[13] Y. Yamashita and K. Ueda, Phys. Rev. Lett. **85**, 4960 (2000).

[14] S.-H. Lee, C. Broholm, T. H. Kim, W. Ratcliff II, and S.-W. Cheong, Phys. Rev. Lett. **84**, 3718 (2000).

[15] A. B. Sushkov, O. Tchernyshyov, W. Ratcliff, S. W. Cheong, and H. D. Drew, Phys. Rev. Lett. **94**, 137202 (2005).

[16] J. H. Chung, M. Matsuda, S. H. Lee, K. Kakurai, H. Ueda, T. J. Sato, H. Takagi, K. P. Hong, and S. Park, Phys. Rev. Lett. **95**, 247204 (2005).

[17] W. Baltensperger and J. S. Helman, Helv. Phys. Acta **41**, 668 (1968).

[18] W. Baltensperger, J. Appl. Phys. **41**, 1052 (1970).

[19] P. Brüesch and F. D. Ambrogio, Phys. Status Solidi B **50**, 513 (1972).

[20] S. Massidda, M. Posternak, A. Baldereschi, and R. Resta, Phys. Rev. Lett. **82**, 430 (1999).

[21] C. J. Fennie and K. M. Rabe, Phys. Rev. Lett. **96**, 205505 (2006).

[22] J. Hemberger, T. Rudolf, H.-A. Krug von Nidda, F. Mayr, A. Pimenov, V. Tsurkan, and A. Loidl, Phys. Rev. Lett. **97**, 087204 (2006).

[23] R. Plumier, J. Phys. (Paris) **27**, 213 (1966).

[24] J. Hemberger, H. A. Krug von Nidda, V. Tsurkan, and A. Loidl, Phys. Rev. Lett. **98**, 147203 (2007).

[25] R. Kleinberger and R. de Kouchkovsky, C.R. Seances Acad. Sci., Ser. A **262**, 628 (1966).

[26] M. Hidaka, N. Tokiwa, M. Fuji, S. Watanabe, and J. Akimitsu, Phys. Status Solidi B **236**, 9 (2003).

[27] T. Rudolf, Ch. Kant, F. Mayr, J. Hemberger, V. Tsurkan, and A. Loidl, Phys. Rev. B **75**, 052410 (2007).

[28] T. Kimura, T. Goto, H. Shintani, K. Ishizaka, T. Arima, and Y. Tokura, Nature (London) **426**, 55 (2003).

[29] For reviews, see M. Fiebig, J. Phys. D **38**, R123 (2005); S.-W. Cheong and M. Mostovoy, Nature Mater. **6**, 13 (2007); A. B. Sushkov, M. Mostovoy, R. V. Aguillar, S. W. Cheong and H. D. Drew, J. Phys.: Condens. Matter **20**, 434210 (2008).

[30] J. Koo, C. Song, S. Ji, J. S. Lee, J. Park, T. H. Jang, C. H. Yang, J. H. Park, Y. H. Jeong, K. B. Lee, T. Y. Koo, Y. J. Park, J. Y. Kim, D. Wermeille, A. I. Goldman, G. Srajer, S. Park, and S. W. Cheong, Phys. Rev. Lett. **99**, 197601 (2007).

[31] Y. Yamasaki, S. Miyasaka, Y. Kaneko, J. P. He, T. Arima, and Y. Tokura, Phys. Rev. Lett. **96**, 207204 (2006).

[32] H. Katsura, N. Nagaosa, and A. V. Balatsky, Phys. Rev. Lett. **95**, 057205 (2005).

[33] I. A. Sergienko and E. Dagotto, Phys. Rev. B **73**, 094434 (2006).

[34] M. Mostovoy, Phys. Rev. Lett. **96**, 067601 (2006).

[35] H. Murakawa, Y. Onose, K. Ohgushi, S. Ishiwata, and Y. Tokura, J. Phys. Soc. Jpn. **77**, 043709 (2008).

[36] D. M. Tobbens, N. Stüßer, K. Knorr, H. M. Mayer, and G. Lampert, Mater. Sci. Forum **378-381**, 288 (2001).

[37] J. Rodriguez-Carvajal, Physica B **192**, 55 (1993).

[38] A. N. Fitch and J. Res, NIST Spec. Publ. **109**, 133 (2004).

[39] J. Akimitsu, K. Siratori, G. Shirane, M. Iizumi, and T. Watanabe, J. Phys. Soc. Jpn., **44**, 172 (1975).

[40] R. Plumier, M. Lecomte, A. Miédan-Gros, and M. Sougi, Phys. Lett. **55A**, 239 (1975).

[41] A. Krimmel, M. Mucksch, V. Tsurkan, M. M. Koza, H. Mutka, C. Ritter, D. V. Sheptyakov, S. Horn, and A. Loidl, Phys. Rev. B **73**, 014413 (2006).

[42] D. Bergman, J. Alicea, E. Gull, S. Trebst, and L. Balents, Nat. Phys. **3**, 487 (2007).

[43] M. Hamedoun, A. Wiedenmann, J. L. Dormann, M. Nogues, and J. Rossat-Mignod, J. Phys. C **19**, 1783 (1986); **19**, 1801 (1986).

[44] S.-H. Lee, G. Gasparovic, C. Broholm, M. Matsuda, J.-H. Chung, Y. J. Kim, H. Ueda, G. Xu, P. Zschack, K. Kakurai, H. Takagi, W. Ratcliff, T. H. Kim, and S.-W. Cheong, J. Phys. Condens. Matter **19**, 145259 (2007).

[45] W. C. Hamilton, Phys. Rev. **110**, 1050 (1958).